Morphological Evolution of Nanoparticles in Diffusion Flames: Measurements and Modeling

Y. Xing, D. E. Rosner, Ü. Ö. Köylü and P. Tandon
Yale University, Dept. of Chemical Engineering, High Temperature Chemical Reaction Engineering Laboratory, New Haven, CT 06520

The morphological evolution of flame-generated "primary" spherules and inorganic aggregates was studied at low particle volume fractions [$O(10^{-1}$ ppm)] in a well-defined/characterized laminar nonpremixed combustion environment which produces particle heating rates of 10^4 K/s. Pure Al_2O_3 particles synthesized in an $Al(CH_3)_3$ (TMA-) seeded atmospheric pressure laminar counterflow diffusion flame "fueled" with $CH_4/O_2/N_2$ were used as the model material/combustion system. Experimental techniques included spatially resolved laser light scattering (LLS) and thermophoretic sampling/transmission electron microscopy. Local aggregate morphology was characterized in terms of spherule ("grain") size, aggregate size, aggregate shape and fractal structure. Effects of flame temperature and TMA concentrations on particle inception location, sizes and morphology studied systematically were interpreted based on parallel theoretical studies. LLS signals and TEM images show particle/aggregate size and morphology evolution as a result of two competing rate processes. Mean spherule diameters prior to high-temperature coalescence are explained in terms of the strong size dependence of nanoparticle restructuring kinetics due to surface melting, even at 500 K. Mean fractal aggregate sizes reached only 15–27 spherules near a local temperature of only 1,250 K. Final particulate products were isolated spherical particles resulting from complete "collapse" of the aggregates in an interval of only 24 ms immediately upstream of the maximum gas temperature (2,280 K). Experimental results are compatible with the characteristic times governing each participating "unit" rate process. Some of these methods can be applied in controlling the larger-scale synthesis of valuable nanopowders and guide rational extensions into the domain of turbulent nonpremixed combustors generating ultrafine particles of tailored composition and morphology at high mass loadings.

Introduction

Inorganic particles produced during combustion are frequently comprised of coagulated spherules often partially sintered due to high temperatures (Helble and Sarofim, 1989; Koch and Friedlander, 1990). The resulting aggregates can be quite different in their morphologies, sizes, and specific surface areas according to the flame conditions under which they are generated and processed. In the case of flame-generated Al_2O_3 particles considered below, the spherule formation process could not be spatially resolved, but at gas temperatures between about 400 K and 1,500 K, particle morphology and size evolution is dominated by aggregate-aggregate Brownian coagulation, leading to tenuously-structured aggregates well described using fractal concepts (Megaridis and Dobbins, 1990; Köylü et al., 1995). However, these coagulating aggregates find themselves in a local environment which is heating up at rates which exceed 10,000 K/s. When the temperature level is high enough (ca. > 1,500 K in the present case) such aggregates undergo surface-en-

Correspondence concerning this article should be addressed to D. E. Rosner.
Current addresses of: Ü. Ö. Köylü, Dept. of Mechanical Engineering, Florida International University, Miami, FL; P. Tandon, Dept. of Chemical Engineering, University of Pennsylvania, Philadelphia, PA 19104.

ergy-driven restructuring processes leading to more compact morphologies. Because particle morphology and aggregate mass-, momentum- and energy-transport properties are interrelated (Tandon and Rosner, 1996), it is important to understand not only the formation of spherules and aggregates but also their *morphological evolution* in flames. The principal objective of the present work is to gain a quantitative understanding of the factors governing primary spherule size and the morphological evolution of flame-generated aggregates in a well-defined/characterized laminar nonpremixed combustion environment, using the experimental techniques of spatially resolved LLS, thermophoretic sampling, TEM image analysis and ancillary particle thermophoresis-based techniques (McEnally et al., 1997; Köylü et al., 1997). Al_2O_3 particles synthesized in an $Al(CH_3)_3$ (TMA-) seeded atmospheric pressure steady laminar CDF (Dixon-Lewis, 1990) were used as the model material/combustion system (Xing et al., 1996a,b) for several reasons: (1) the kinetics of fine particle nucleation (from the rapid hydrolysis of trimethyl aluminum (TMA)) is far simpler than, say, the formation of carbonaceous soot from even simple hydrocarbon vapor fuels via polycyclic aromatic hydrocarbon intermediates (Frenklach and Wang, 1990); (2) the thermophysical properties of pure macroscopic Al_2O_3(c) are relatively well known, even at the high temperatures achieved here; (3) ultrafine particles of Al_2O_3(c) and other metal oxides are of technological importance in many areas, including materials synthesis (Ulrich, 1984; Pratsinis, 1997), power generation (Rosner and Tandon, 1995), and chemical propulsion (Sambramurthi and Alvarado, 1996); (4) laminar CDF structure is not only amenable to detailed experimental probing, but also comprehensive theoretical modeling via the solution of coupled ordinary differential equations (ODEs) (Dixon-Lewis, 1990) or integro-ODEs (Zacharaiah and Semerjian, 1989; Hall et al., 1997; this work, cf. Figure 9). Finally, as noted below, we view this work as a logical and necessary step in the understanding of particle formation/evolution in *turbulent* nonpremixed synthesis flames—that is, an important evolving branch of *sol reaction engineering*.

In keeping with these objectives, the effects of temperature, residence time, and precursor TMA concentration on local spherule sizes and aggregate morphology are being investigated systematically and compared with quantitative theoretical predictions. Indeed, while the present environment is admittedly more complicated to study than highly idealized laminar duct-in-furnace steady flow reactors, it will be seen that this steady CDF environment not only lends itself to experimental probing and a quantitative model of the detailed *structure* of two-phase synthesis flames, but, also, through extended flamelet concepts (Bilger, 1988; Peters, 1984) or alternative microflow models (Magel et al., 1996), our methods/results will open the door to a better understanding of particle production/restructuring in initially nonpremixed *turbulent* diffusion flame reactors.

Experimental Methods

Because many of the relevant experimental techniques are described in Xing et al. (1996) and Köylü et al. (1995), this section only outlines the most essential features. A water-cooled CDF reactor was constructed and used to synthesize

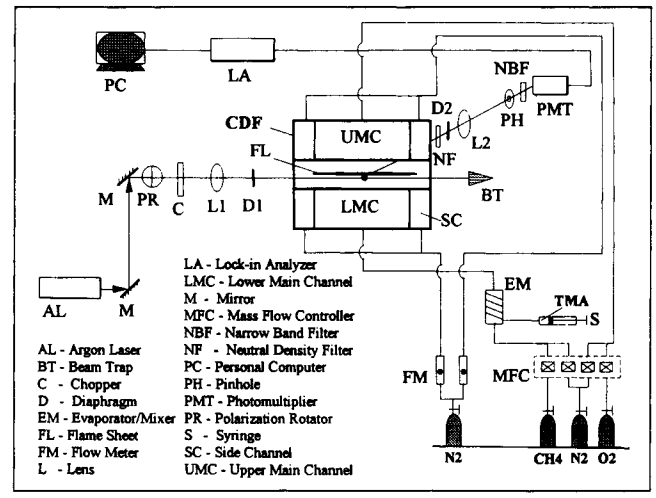

Figure 1. Rectangular counterflow diffusion flame (CDF) burner assembly and associated systems (after Xing, 1997).

ultrafine inorganic particles with specific surface areas exceeding 100 m^2/g. The bench-scale reactor consisted of two opposed identical rectangular slots (64 mm × 13 mm) (see Figure 1 for burner, feed system and associated instrumentation) separated by 15 mm (cf. Chung and Katz, 1985). Methane was used as the gaseous fuel and oxygen was the oxidizer, both diluted by nitrogen. Combustion gas-flow rates were selected such that suitable flat horizontal flames (FL) could be stabilized for studying not only nanospherule formation, but also the *morphological evolution* of alumina aggregates. Liquid TMA particle precursor was fed into an evaporator using a calibrated syringe/piston pump at rates corresponding to alumina particle volume fractions between about 0.07 and 0.3 ppm, that is, deliberately low enough to negligibly alter the CH_4/O_2 counterflow host flame characteristics. For the cases shown below, flame conditions were: fuel/air momentum flux ratio 3.5, equivalence ratio 0.68, and nominal strain rate 13 s^{-1}. Alumina particles were formed by TMA hydrolysis on the fuel side of the flame, coagulated among themselves to form fractal aggregates, moved on to higher temperature regions and ultimately through the flame (FL), only to be ejected at/before the plane marked: *particle stagnation plane* (PSP) (Gomez and Rosner, 1993; Miquel, 1995), estimated to be only about 1.4 mm, beyond the gas stagnation plane (GSP) ($v_z(z_{GSP}) = 0$). As quantified below, this history causes the morphology of the particles to change dramatically due to the high prevailing flame temperatures [thermocouple-measured; radiation-corrected (Figure 2)], T_{FL} = 2,280 K, somewhat lower than the equilibrium melting point (about 2,330 K) of bulk alumina.

A thermophoretic particle sampling technique (Dobbins and Megaridis, 1987), unbiased with respect to aggregate size and morphology (Rosner et al., 1991), was used to extract and examine alumina particles from the reactor at four equally spaced positions along the vertical z axis ($x = 0$, $y = 0$). The morphologies of alumina aggregates (Figures 3–5, giving, respectively, TEM images, spherule and equivalent aggregate diameters and fractal dimension) were obtained using TEM photographs and image processing software. De-

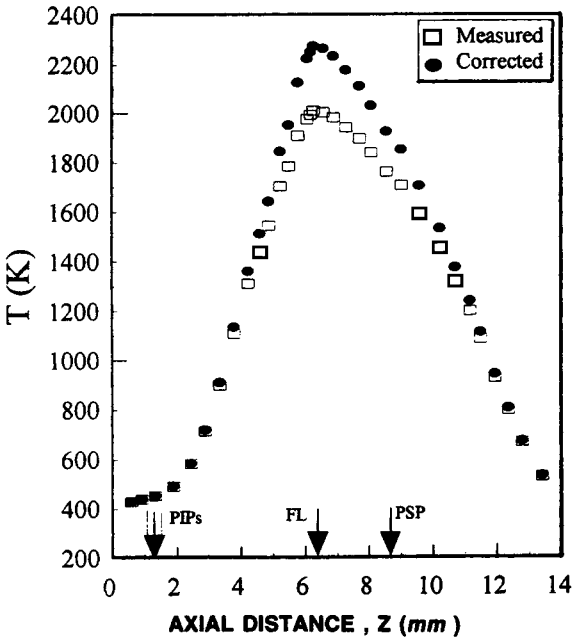

Figure 2. Thermocouple-measured/inferred gas temperatures in the reference CH_4/O_2 counterflow flame (FL).

Fuel/air momentum flux ratio 3.5; equivalence ratio 0.68; and nominal strain rate 13 s^{-1} (after Xing et al., 1996a).

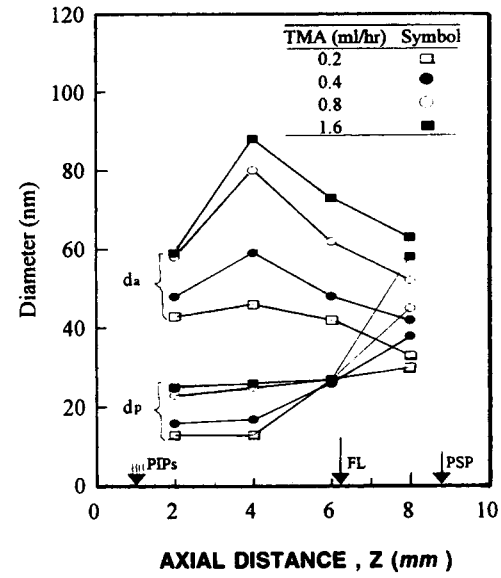

Figure 4. Observed mean spherule (primary particle) diameter (Xing et al., 1996a) and TEM area-equivalent aggregate diameter as functions of position z in counterflow diffusion flame for various TMA seed levels.

tails of these image analysis procedures are presented elsewhere (Köylü et al., 1995). The particle inception plane (PIP) locations, the coagulation and restructuring processes, and the particle stagnation (ejection) plane (PSP) were also monitored using nonintrusive laser light scattering (LLS) techniques at a wavelength of 514.5 nm (Figures 1 and 6).

Results and Discussion

Spherule diameters measured directly from digitized TEM (micrographs) by detecting the profiles of the constituent primary particles are shown in Figure 3 at four TMA seed levels (liquid pumping rates). Even at our first sampling location ($z = 2$ mm) beyond PIP, Al_2O_3 spherules are ≥ 10 nm dia. and are found in relatively small aggregates ($10 < N < 19$ spherules, depending on the seed level). As expected for a

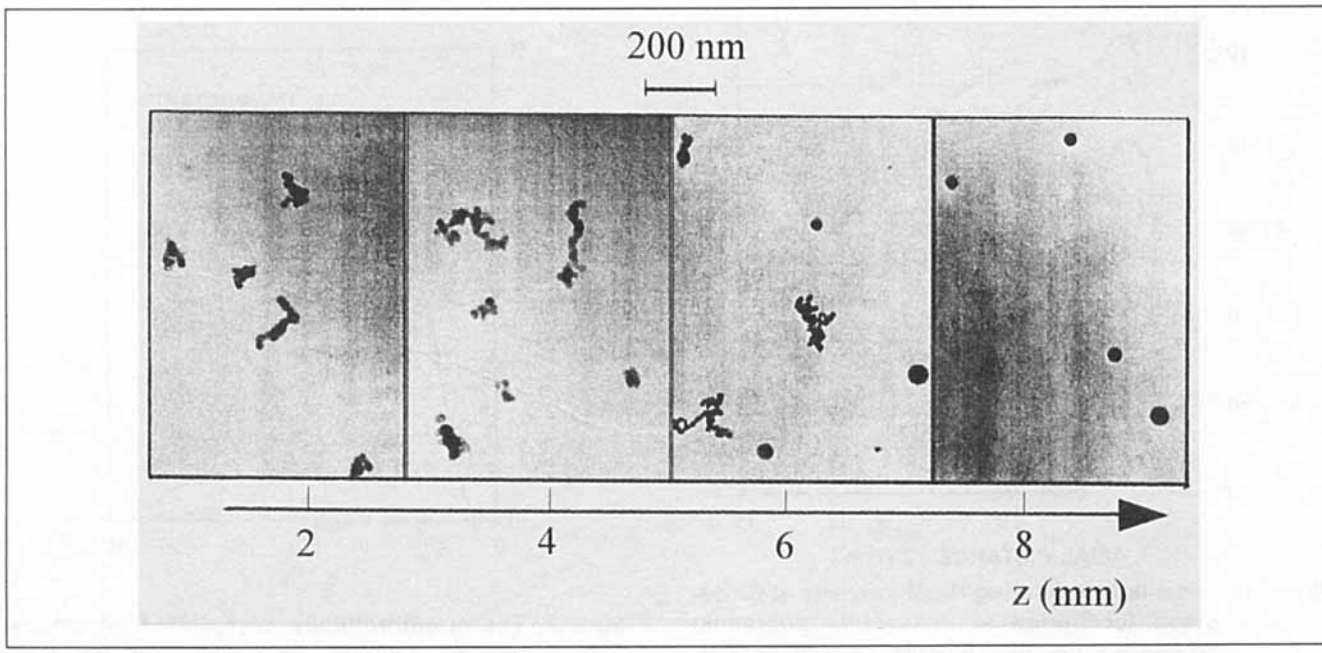

Figure 3. TEM photographs of thermophoretically extracted particles from 4 positions along the axis of the laminar counterflow diffusion flame (after Xing et al., 1996a).

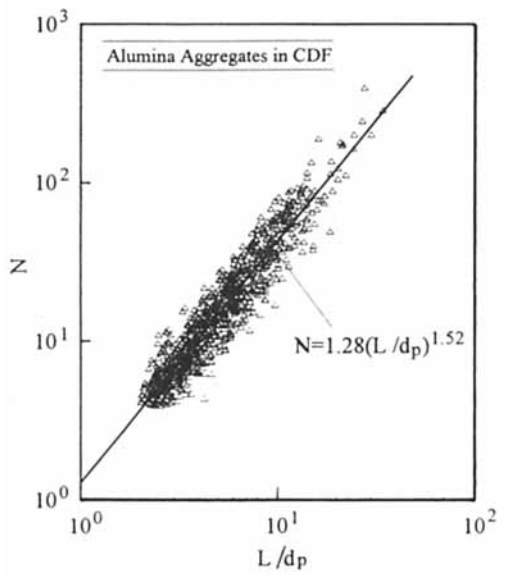

Figure 5. Number of spherules in aggregate vs. maximum projected (TEM) length (in spherule diameters) for aggregates thermophoretically extracted from TMA-seeded counterflow diffusion flame at $z = 2$ and 4 mm (after Xing et al., 1996a).

nearly diffusion-controlled TMA hydrolysis reaction, PIP locations moved closer to the flame zone (source of back-diffusing $H_2O(g)$) at the higher seed levels (see Figure 6). As discussed below, the low temperatures at the location of Al_2O_3-formation from TMA hydrolysis (< 500 K) is responsible for the small spherule diameters (and correspondingly high specific surface areas) observed in these experiments.

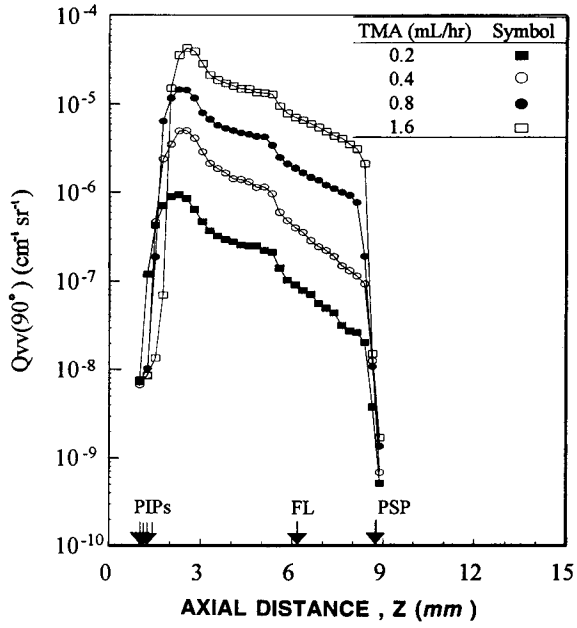

Figure 6. Laser light scattering (LLS) intensity at 90 degrees (converted to volumetric differential cross-sections) as a function of vertical position z in the CDF for various TMA seed levels (after Xing et al., 1997).

While we were not able to spatially resolve the spherule formation process in these experiments, in Xing and Rosner (1997) we quantitatively consider the size dependence of the near-PIP restructuring *rate* processes and its implications for the observed trends in spherule (grain) size (Figure 4). It appears that the observed small spherule sizes (say, at $z = 2$ mm) are the result of the size-dependence of nanosphere coalescence at these low temperatures (Xing and Rosner, 1997), that is, beyond the observed size (approximately 13 nm at a TMA-feed rate of 0.2 mL/h) restructuring with the help of nanosphere "surface melting" at ca. 500 K, it is unable to keep up with spherule Brownian coagulation. This remains true during aggregate formation even in the rising temperature host-gas environment, at least until above 1,500 K. Also shown in Figure 4 are the corresponding trends in the *aggregate* area-equivalent diameter (d_a) calculated from: $(4A_a/\pi)^{1/2}$ using the projected area (A_a) of each sampled aggregate (directly measured from 2-D TEM images). Increased TMA-seed level is also seen to lead to larger aggregate sizes. Log-normal distributions (Figure 7) have been observed for d_a with geometric standard deviations in the range 1.43–1.90. Prior to their restructuring in the higher temperature zone of our CDF, the alumina aggregates are observed to lie mostly in the projected area-equivalent diameter range: 30 nm to 90 nm that can be treated as being in the near free-molecular regime in our present atmospheric pressure flames. Thus, d_a is approximately the *mobility diameter* of the $D_f < 2$ alumina aggregates in these combustion environments (Sorensen et al., 1992; Rogak et al., 1993). In the present case we estimate (see below) that the number N of spherules in an aggregate of area-equivalent diameter scales like $N \sim (d_a)^{2.18}$ (Köylü et al., 1995) so that the N-distribution probability density function $pdf(N)$ is also approximately log-normal, with σ_g-values near 3 (cf. 3.5, the estimated self-preserving spread, σ_g of $D_f \approx 1.6$ fractal ag-

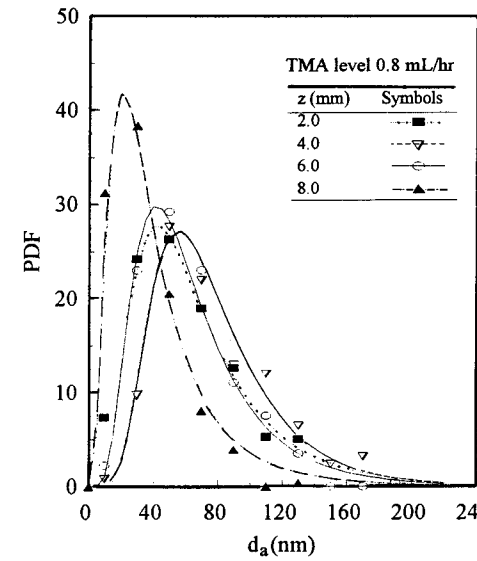

Figure 7. Thermophoretically sampled/TEM image-derived alumina aggregate projected area-equivalent size distributions at several positions within the flame.

gregate populations (see below) in the free-molecule Brownian coagulation domain; Tandon, 1995). Even if all spherules in such aggregates were the same diameter this $pdf(N)$ entering the restructuring zone would be associated with a spread in the expected high-temperature restructuring times —however, this particular effect is quite small because of the expected weak dependence of restructuring time on N (Tandon and Rosner, 1996).

As mentioned above, prior to the onset of high-temperature sintering, the thermophoretically sampled Al_2O_3 aggregates (at $z = 2$ and 4 mm) exhibited tenuous structures that can be conveniently described as *mass fractal*, in the sense that: $N = k_g \cdot (R_g/a)^{D_f}$, where N is the number of individual spherules in the aggregate, k_g is the prefactor, R_g the 3-D radius of gyration about the aggregate center-of-mass, a, the local mean spherule radius, and the exponent D_f is the so-called fractal "dimension." Since R_g is not directly accessible from the unidirectional projected TEM images, the fractal dimension and prefactor were obtained using the practical methods proposed/implemented by Köylü et al. (1995), with the results shown in Figure 3. Values of k_g and D_f for these Al_2O_3-aggregates were found to be in the same ranges as for many other flame-generated high-area materials, including carbonaceous soot, as shown in Table 1 (Köylü et al., 1995; Megaridis and Dobbins, 1990). However, an interesting finding is that these flame-generated aggregates differ from diffusion-limited cluster-cluster computer-simulated aggregates (Meakin et al., 1989; Wu and Friedlander, 1993) in two potentially important respects—viz., their prefactors k_g are larger (2.2 cf. 1.3; see e.g., Köylü et al., 1995), and they are *self-affine* rather than self-similar, tending toward larger *aspect ratio* at larger N-values (Neimark et al., 1996). The radiative and transport property implications of these systematic differences are presently under investigation.

Significant morphological changes for alumina particles evidently occurred between the PIP and PSP in this flame. This was clear in our TEM images (see, e.g., Figure 3) and can be quantified *via* trends observed in the particle *shape factors* $C_{sf} = P^2/(4\pi A_a)$, where P is the *perimeter* of the projected ($D_f < 2$) aggregate TEM image (Figure 8). Changes in this parameter reveal the combined effects of coagulation and sintering on the morphology of the alumina aggregates—trends now a focus of our modeling efforts (see below). Near PIP coagulation presumably starts from a burst of quasi-spherical monomers, with $C_{sf} \to 1$. As low temperature spherule Brownian coagulation proceeds, the nanospherules

Table 1. Morphological Descriptors* for Inorganic and Organic Flame-Generated Aggregates**

	Carbonaceous Soot	Alumina**
Fractal dimension, D_f	1.7 ± 0.1	1.5 ± 0.1
Fractal pre-factor, k_g	2.4	2.2

*Values of D_f and k_g appearing in: $N = k_g \cdot (R_g/(d_p/2))^{D_f}$.
**Based on laboratory measurements of over 100 Al_2O_3 aggregates thermophoretically extracted from a well-characterized TMA-seeded methane laminar counterflow flame, values of the parameters D_f and k_g are remarkably close to those characterizing carbonaceous soot aggregates in hydrocarbon/air flames. Underlying cause is the similarity between the aggregate-aggregate Brownian coagulation mechanism in the two cases (under flame conditions of negligible restructuring or spherule growth from the vapor).

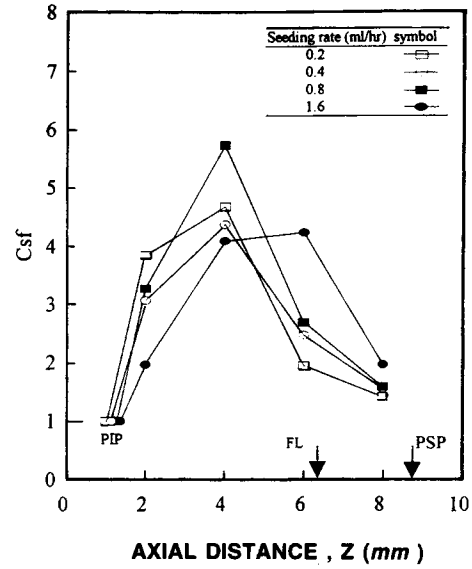

Figure 8. Alumina aggregate *shape factor* (sphericity) C_{sf} via TEM image analysis as a function of axial position in TMA seeded methane-fueled laminar counterflow diffusion flame.

grow until their coalescence rate cannot keep up with the spherule coagulation rate and small aggregates are formed with mean C_{sf} values passing through a maximum (here near 6), downstream of which (for $T_g > 1{,}500$ K) high-temperature sintering effects dominated. Indeed, C_{sf} again approached unity near the particle stagnation (ejection) plane. We have demonstrated (Xing, 1997) using LLS and a recently developed thermocouple response technique (McEnally et al., 1997) that, despite the important role of axial thermophoresis (Gomez and Rosner, 1993), the restructuring process evident in Figures 3, 4, and 8 is associated with an alumina particle *mass* fraction nearly constant and equal to that expected from the aluminum *element* mass fraction (Rosner, 1986) corresponding to the initial TMA seed level. Moreover, the ultimate coalescence of such aggregates during their rapid approach to the flame temperature is expected based on a coagulation model which assumes Brownian coagulation in environments with constant heating rates (of the order of 10,000 K/s). These preliminary simulations which, for simplicity, assumed negligible streamwise diffusion, suggested that this is indeed an environment in which there are *two* disparate locations at which the coalescence rate can keep up with Brownian coagulation (cf. Figure 10)—one at low temperature (due to very small spherule size) and one at high temperature (due to the much higher condensed phase near-surface molecular mobilities) closer to the "bulk" melting temperature.

Our work on the use of 90° laser light scattering data to interpret the *progress* of restructuring is not yet complete (Farias et al., 1996; Xing, 1997), but it is informative and more straightforward to apply LLS-theory to our data both upstream and downstream of the aggregate restructuring zone. This is being done assuming Rayleigh-Debye-Gans "fractal scatterers" upstream, and isolated (but larger) Rayleigh scatterers downstream, since the final products are larger diameter compact spherical particles (resulting from complete col-

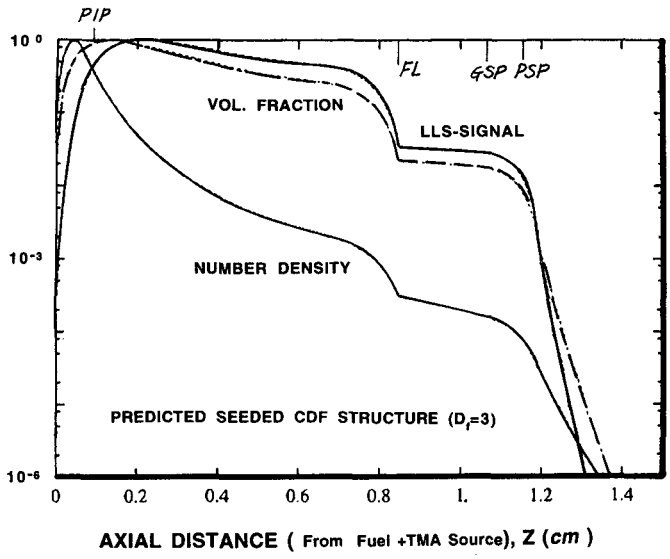

Figure 9. Predicted profiles (normalized) of light scattering intensity, alumina particle volume fraction and number density in a TMA-seeded laminar CDF including axial Brownian diffusion and thermophoresis if all particles coagulated and rapidly coalesced downstream of the hydrolysis (PIP-) location (near 0.1 cm).

Fuel/air momentum flux ratio 3.5; equivalence ratio 0.68; and nominal strain rate 13 s^{-1}.

lapse of aggregates; see below) observed near PSP at all seed levels. Figure 6 shows the LLS transition between these two restructuring zone asymptotes ($D_f = 1.6$, 3) as modified by volume fraction changes associated with axial thermophoresis (cf. Figure 9). Moreover, judging by the apparent "widths" of the restructuring zone (Figures 6 and 8) the total time required to complete restructuring (evidently at most about 24 ms, the time for each particle to traverse the axial distance is between about 4.1 mm to 5.8 mm) is rather *insensitive* to seed level, despite the fact that the mean spherule diameter in the initial aggregates differed by a factor of about two over this eightfold change in seed level (Figure 4). Assuming that the LLS signal is sufficiently sensitive to the onset and termination of restructuring, this apparent insensitivity of restructuring time to seed level, at first sight, seems inconsistent with a surface diffusion sintering mechanism (see Xing et al., 1996, and next section). In this connection, the abovementioned $C_{sf}(z)$ trends do suggest a noticeably longer restructuring time at the largest seed levels (that is, at larger initial spherule diameters), roughly in accord with expectations based on a surface-energy driven *viscous flow* isothermal restructuring mechanism. However, in these CDF-experiments aggregate restructuring is occurring in a rapidly rising temperature environment. Because of the Arrhenius-like dependence of condensed phase diffusivities this will tend to suppress the spherule diameter dependence since larger spherules will inevitably experience higher temperatures. Thus, our present LLS and TEM measurements are not inconsistent with *surface-diffusion* as the dominant aggregate restructuring mechanism above 1,500 K. These, and related matters, discussed briefly below, will be the subject of our follow-on research.

Sol-Reaction-Engineering Aspects

Aggregate evolution observed here is evidently the result of two identifiable rate processes: aggregate coagulation and intra-aggregate coalescence. Accordingly, it has been instructive to examine the *characteristic times* associated with these, and other, possibly relevant counterflow flame unit processes (see, for example, Rosner, 1986; Xing et al., 1996a) and Figure 5, using $\log_{10}$ (time) vs. reciprocal absolute temperature coordinates). These estimates revealed that the TMA vapor hydrolysis time (less than 10^{-2} ms) and the aggregate momentum response time (< 1 ms) are negligible compared to the characteristic flow (residence) time in these flames (> 10 ms). Thus, we have succeeded in creating a well-defined flame environment in which the chemical processes of methane oxygen combustion (O(1 ms) (O is the order-of-magnitude operator) based on the sharp peak in Figure 2) and alumina particle precursor formation via TMA hydrolysis can be considered instantaneous on the time scale of the physical processes of particle Brownian coagulation and surface-energy driven aggregate restructuring, of principal concern here. Moreover, the estimated time between aggregate-aggregate coagulation events crossed the estimated characteristic grain surface-diffusion sintering time (nearly a straight line on these coordinates) somewhat below 2,000 K. At any one seed level, this crossover temperature is consistent with the evidence for aggregate pre-flame collapse from both our light scattering results (Figure 4) and the abovementioned TEM-image-derived shape factors C_{sf}. Moreover, the weak dependence of restructuring time on initial spherule diameter (which at first sight might argue for a viscous flow model) is probably the result of restructuring by surface diffusion occurring in a rapidly rising temperature environment (Rosner et al., 1997). (Despite our pre-flame heating rates in excess of 10,000 K/s, these flame-generated nano-particles are small enough to have no difficulty "tracking" these local temperatures (see Xing et al., 1996a). In terms of molecular mixing theory (Peters, 1984; Bilger, 1988) the scalar dissipation rates in our flames are of the order of 10 s^{-1}.) Incidentally, had the spherules behaved throughout like ordinary supercooled viscous alumina, we estimated that aggregate collapse via surface-tension driven viscous flow (Koch and Friedlander, 1990; Tandon and Rosner, 1996) should have occurred even below 700 K (see dashed nearly straight line of Figure 10). Thus, despite their external shape, evidently these nano-spherules do *not* behave like homogeneous spherules of viscous supercooled molten alumina, even above 1,500 K. Evidently, spherules much smaller than those observed at $z = 2$ mm *were* able to restructure at even below 500 K, probably due to the phenomenon of "surface melting" (Xing and Rosner, 1996). This is indicated by the nearly straight line which intersects the characteristic coagulation time shortly after PIP (Figure 10).

Development of a more comprehensive mathematical model of particle size/morphological evolution in dilute TMA-seeded laminar CDFs is underway in our research group (Rosner et al., 1995, 1996, 1997). As a first step (briefly described above), we have computed the expected CDF particle normalized light scattering profile if: (a) coalescence were rapid enough to keep all Brownian coagulated particles spherical ($C_{sf} = 1$) in the Rayleigh regime (Figure 9, which also contains the corresponding profiles of particle number

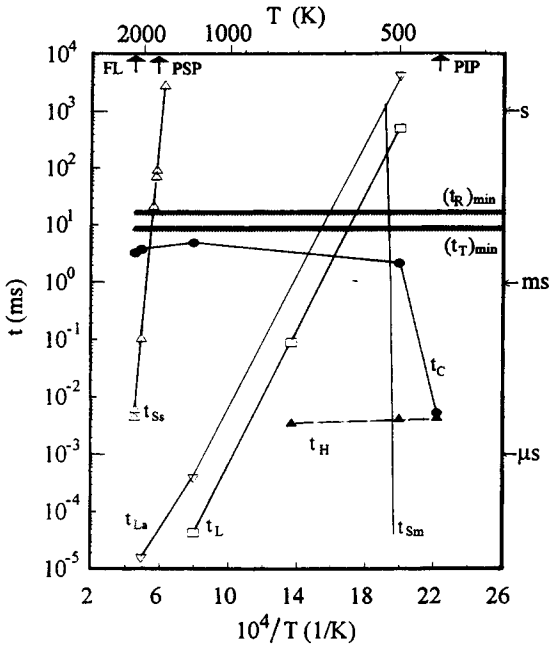

Figure 10. Relevant *characteristic times* (log-scale) as a function of $10^4/T_g$ for comparing the relative importance of simultaneous chemical and physical rate processes in a methane/oxygen CDF (after Xing et al., 1996a), but including estimates for ordinary supercooled liquid (*L*) alumina, and surface diffusion across nanometer-range spherules with *surface melting* (Sm) near PIP (Xing and Rosner, 1996; Xing, 1997).

Also shown are minimum local times associated with appreciable fractional changes in axial velocity or temperature (after Xing et al., 1996a).

density and volume fraction, and (b) (not shown in Figure 9) the coalescence rate were always negligible, leading to aggregates of nearly constant fractal dimension (ca. 1.6) (cf. Figure 5). For this purpose, an equal molecular diffusivity nonpremixed "flame sheet" approximation is adequate to generate the host gas flow field (see, for example, Rosner, 1986). Comparing available results (Figure 9, Part a) with our experimental LLS measurements (Figure 6), it is observed that some of the principal features are similar. A more detailed quantitative examination of these thermophoretically modified two-phase laminar CDF-structures (see, also, Gomez and Rosner, 1993; Garcia-Ybarra and Castillo, 1997) will be part of our future research, along with their expected implications for *turbulent* nonpremixed synthesis flames.

Particle population balance methods (see, for example, Zacharaiah and Semerjian, 1989; Hall et al., 1997), but which allow for the observed "arrest" in spherule size, fractal aggregate formation upon Brownian coagulation (Tandon, 1995), and finite-rate intra-particle sintering (Koch and Friedlander, 1990; Xiong and Pratsinis, 1993; Tandon and Rosner, 1997) in such variable density CDFs with non-negligible streamwise (Brownian + thermophoretic) diffusion are currently being implemented, using the unique thermophysical/transport properties of fractal aggregates (Rosner and Tandon, 1994; Tandon and Rosner, 1995, 1996). When combined with the anticipated light scattering properties of aggregates containing such partially sintered particles (Köylü et al., 1995, 1997), our methods will provide instructive predictions to compare in detail with experimental data of the type shown in Figures 6 and 8. We view this laminar, dilute two-phase CDF laboratory research as a necessary prelude to understanding *turbulent nonpremixed* nanoparticle synthesis flames of industrial interest.

Conclusions and Implications

We are using lightly seeded laminar counterflow diffusion flames as prototypical systems to understand the competition between Brownian coagulation and surface energy-driven coalescence-sintering in determining the size and morphology of flame-generated metal oxides. The experimental and theoretical methods/results described above, pertinent to alumina particle volume fractions of the order of 10^{-1} ppm in atmospheric pressure diffusion flames, have led us to the following conclusions:

(a) As desired, in these highly nonisothermal steady laminar flame environments the *chemical* processes of methane oxygen combustion and alumina particle precursor formation *via* TMA hydrolysis can be considered instantaneous on the time scale of the *physical* processes of particle Brownian *coagulation* and surface-energy driven aggregate *restructuring*, of primary concern here.

(b) Spatially-resolved static laser light scattering (LLS) combined with local thermophoretic sampling/TEM image analysis and thermocouple response techniques are able to economically and quantitatively track the dynamics of the morphological evolution of alumina nano-sphere assemblies in steady atmospheric pressure counterflow diffusion flames at strain rates $|dv_z/dz|$, and scalar dissipation rates of the order of $10\ s^{-1}$, and preflame heating rates which exceed 10,000 K/s.

(c) The observed sequence of alumina nano-spherule formation, fractal aggregate formation above a threshold spherule size, and ultimate aggregate collapse appears to be consistent with the size- and temperature-sensitive competition between Brownian coagulation and surface-energy driven restructuring kinetics, *provided one accounts for the non-macroscopic properties of nano-particles* and the changing morphology of the coagulating particles.

(d) Despite the observed weak (at most linear) dependence of aggregate restructuring time (ca. tens of milliseconds) on initial spherule diameter (via changes in seed level) suggested by our shape-factor results (Figure 8), the alumina aggregate restructuring mechanism above 1,500 K is probably *not* viscous flow-like. While the *surface-diffusion* mechanism would lead to restructuring times proportional to $(d_1)^4$ in an *isothermal* environment, this is not observed in the (present) case of rapidly rising temperatures. Indeed, the present CDF environment is ideal to restructure aggregates comprised of disparate sized spherules in nearly the same time.

(e) Prior to restructuring during their rapid approach to the flame temperature, Al_2O_3 aggregates extracted from these $Al(CH_3)_3$-seeded CDFs, when compared with *organic "soot" aggregates* from a wide variety of hydrocarbon/air flames, appear to be *morphologically similar* with respect to both fractal dimension $D_f \approx 1.6$ and prefactor $k_g \approx 2.2$—cf. Table 1.

Information on alumina *spherule microstructure* and *spherule surface characteristics* are important objectives of studies in progress. The principles/laws that emerge from this combined bench-scale experimental and modeling research effort are expected to find applications in controlling the large-scale synthesis of valuable nano-powders, as well as facilitate rational extensions into the industrially significant domain of highly-loaded (Rosner and Park, 1988; Park and Rosner, 1989), *turbulent*, nonpremixed combustors (Pope, 1990, 1991; Fox, 1992) generating ultrafine particles of tailored size, composition, and morphology.

Acknowledgments

These closely coupled experimental and theoretical studies were supported in part by AFOSR grant No. F49620-97-1-0266 (Dr. J. M. Tishkoff, Technical Monitor) and by the Yale HTCRE Lab *Industrial Affiliates*: Du Pont and ALCOA. The authors also acknowledge the helpful contributions of D. Albagli, A. Gomez, J. Fernandez de la Mora, T. Farias, and C. McEnally.

Literature Cited

Bilger, R. W., "The Structure of Turbulent Non-Premixed Flames," *Proc. Int. Symp. on Combustion*, Comb. Inst., Pittsburgh, p. 475 (1988).

Cai, J., N. Lu, and C. M. Sorensen, "Analysis of Fractal Cluster Morphology Parameters: Structural Coefficient and Density Autocorrelation Function Cut-off," *J. Colloid Int. Sci.*, **171**, 470 (1995).

Chung, S., and J. L. Katz, "The Counterflow Diffusion Flame Burner: A New Tool for the Study of the Nucleation of Refractory Compounds," *Comb. & Flame*, **61**, 271 (1985).

Dixon-Lewis, G., "Structure of Laminar Flames," *Proc. Int. Symp. on Combustion*, Comb. Inst., Pittsburgh, p. 305 (1990).

Dobbins, R. A., and C. M. Megaridis, "Morphology of Flame-Generated Soot as Determined by Thermophoretic Sampling," *Langmuir (ACS)*, **3**, 254 (1987).

Farias, T. L., M. G. Carvalho, Ü. Ö. Köylü, Y. Xing, and D. E. Rosner, "Light Scattering Analysis of Inorganic Oxide Aggregates Undergoing Restructuring in Flames," Paper No. 4B1, AAAR Conf., Orlando, FL (Oct. 14–18, 1996).

Fox, R. O., "Computation of Turbulent Reacting Flows: First Principles Macro/Micro-mixing Models Using Probability Density Function Methods," *Chem. Eng. Sci.*, **47**, 2853 (1992).

Frenklach, M., and H. Wang, "Detailed Modeling of Soot Particle Nucleation and Growth," *Proc. Int. Symp. on Combustion*, Comb. Inst., Pittsburgh, p. 1559 (1990).

Garcia-Ybarra, P., and D. E. Rosner, "Thermophoretic Properties of Nonspherical Particles and Large Molecules," *AIChE J.*, **35**(1), 139 (1989).

Garcia-Ybarra, P., and J. L. Castillo, "Mass Transfer Dominated by Thermal Diffusion in Laminar Boundary Layers," *J. Fluid Mech.*, **336**, 379 (1997).

Gomez, A., and D. E. Rosner, "Thermophoretic Effects on Particles in Counterflow Laminar Diffusion Flames," *Comb. Sci. Tech.*, **89**, 335 (1993).

Hall, R., M. D. Smooke, and M. Colket, "Coupled Modelling of Soot Formation and Thermal Radiation in Counterflow Diffusion Flames," *Physical and Chemical Aspects of Combustion— A Tribute to Irvin Glassman*, Comb. Sci. Tech. Book Ser., Gordon and Breach, in press (1997).

Helble, J. J., and A. F. Sarofim, "Factors Determining the Primary Particle Size of Flame-Generated Inorganic Aerosols," *J. Colloid Int. Sci.*, **128**, 348 (1989).

Katz, J. L., and C.-H. Hung, "Ultrafine Refractory Particle Formation in Counterflow Diffusion Flames," *Comb. Sci. Tech.*, **82**, 169 (1992).

Koch, W., and S. K. Friedlander, "The Effect of Particle Coalescence on the Surface Area of a Coagulating Aerosol," *J. Colloid Interf. Sci.*, **82**, 169 (1990).

Köylü, Ü. Ö., Y. Xing, and D. E. Rosner, "Fractal Morphology Analysis of Combustion-Generated Aggregates Using Angular Light Scattering and Electron Microscope Images," *Langmuir (ACS)*, **11**(12), 4848 (1995).

Köylü, Ü. Ö., G. M. Faeth, T. L. Farias, and M. G. Carvalho, "Fractal and Projected Structure Properties of Soot Aggregates," *Comb. & Flame*, **100**, 621 (1995).

Köylü, Ü. Ö., and G. M. Faeth, "Structure of Overfire Soot in Bouyant Turbulent Diffusion Flames at Long Residence Times," *Comb. & Flame*, **89**, 140 (1992).

Köylü, Ü. Ö., C. S. McEnally, D. E. Rosner, and L. Pfefferle, "Simultaneous Measurements of Soot Volume Fraction and Particle Size/Microstructure in Flames Using a Thermophoretic Sampling Technique," *Comb. & Flame*, **110**(4), 494 (1997).

Köylü, Ü. Ö., "Quantitative Analysis of *In-Situ* Optical Diagnostics for Inferring Particle/Aggregate Parameters in Flames: Implications for Soot Surface Growth and Total Emissivity," *Comb. & Flame*, **109**, 488 (1997).

Magel, H. C., U. Schnell, and K. R. G. Hein, "Simulation of Detailed Chemistry in a Turbulent Combustor Flow," *Proc. Int. Symp. on Combustion*, Comb. Inst., Pittsburgh, p. 67 (1996).

Meakin, P., B. Dunn, and G. W. Mulholland, "Collisions Between Point Masses and Fractal Aggregates," *Langmuir (ACS)*, **5**, 510 (1989).

Megaridis, C. M., and R. A. Dobbins, "Morphological Description of Flame-Generated Materials," *Comb. Sci. Tech.*, **71**, 95 (1990).

McEnally, C. S., Ü. Ö. Köylü, L. Pfefferle, and D. E. Rosner, "Soot Volume Fraction and Temperature Measurements in Laminar Non-Premixed Flames Using Thermocouples," *Comb. & Flame*, **109**, 701 (1997).

Miquel, P. F., "Flame Synthesis of Nano-structured Mixed Oxides and Its Application to the Formation of Catalysts," PhD Diss., Johns Hopkins Univ. (1995).

Miquel, P. F., and J. L. Katz, "Formation and Characterization of Nano-structured V-P-O Particles in Flames: A New Route for the Formation of Catalysts," *J. Mater. Res.*, **9**, 746 (1994).

Neimark, A. V., Ü. Ö. Köylü, and D. E. Rosner, "Extended Characterization of Combustion-Generated Aggregates: Self-Affinity and Lacunarities," *J. Colloid Int. Sci.*, **180**, 590 (1996).

Park, H. M., and D. E. Rosner, "Combined Inertial and Thermophoretic Effects on Particle Desposition Rates in Highly Loaded Dusty Gas Systems," *Chem. Eng. Sci.*, **44**(10), 2233 (1989).

Park, H. M., and D. E. Rosner, "Boundary Layer Coagulation Effects on the Size Distribution of Thermophoretically Deposited Particles," *Chem. Eng. Sci.*, **44**(10), 2225 (1989).

Peters, N., "Laminar Diffusion Flamelets in Non-Pre-mixed Turbulent Combustion," *Prog. Energy Comb. Sci.*, **10**, 319 (1984).

Pope, S. B., "Combustion Modeling Using Probability Density Function Methods. Numerical Approaches to Combustion Modeling," *Numerical Approaches to Combustion Modeling*, E. S. Oran and J. P. Boris, eds., AIAA Press, Washington, DC, p. 349 (1991).

Pope, S. B., "Computations of Turbulent Combustion: Progress and Challenges," *Proc. Int. Symp. on Combustion*, Comb. Inst., Pittsburgh, p. 591 (1990).

Pratsinis, S. E., "Flame Aerosol Synthesis of Ceramic Powders," *Prog. Energy Comb. Sci.*, in press (1997).

Rogak, S. N., R. C. Flagan, and H. V. Nguyen, "The Mobility and Structure of Aerosol Agglomerates," *Aerosol Sci. Tech.*, **18**, 25 (1993).

Rosner, D. E., *Transport Processes in Chemically Reacting Flow Systems*, 3rd printing, Butterworth-Heinemann, Stoneham, MA (1990).

Rosner, D. E., D. W. Mackowski, and P. Garcia-Ybarra, "Size- and Structure-Insensitivity of the Thermophoretic Transport of Aggregated 'Soot' Particles in Gases," *Comb. Sci. Tech.*, **80**, 87 (1991).

Rosner, D. E., D. W. Mackowski, M. Tassopoulos, J. L. Castillo, and P. Garcia-Ybarra, "Effects of Heat Transfer on the Dynamics and Transport of Small Particles Suspended in a Gas," *I/EC-Research (ACS)*, **31**, 760 (1992).

Rosner, D. E., and D. Papadopoulos, "Jump, Slip, and Creep Boundary Conditions at Non-Equilibrium Gas/Solid Interfaces," *I/EC Res. (ACS)*, **35**(9), 3210 (1996).

Rosner, D. E., and P. Tandon, "Diffusion and Heterogeneous Reaction in Large Multi-Particle Aggregates: Calculation and Correlation of 'Accessible' Surface Area," *AIChE J.*, **40**(7), 1167 (1994).

Rosner, D. E., and P. Tandon, "Rational Prediction of Inertially Induced Particle Deposition Rates for a Cylindrical Target in a Dust-Laden Stream," *Chem. Eng. Sci.*, **50**(21), 3409 (1995).

Rosner, D. E., and H. M. Park, "Thermophoretically Augmented Mass, Momentum, and Energy Transfer Rates in High Particle Mass-Loaded Laminar Forced Convection Systems," *Chem. Eng. Sci.*, **43**(10), 2689 (1988).

Rosner, D. E., P. Tandon, and Y. Xing, "Restructuring Kinetics of Multi-spherule Aggregates in Non-isothermal Flame Environments," in press (1997); paper 157h, AIChE Meeting, Los Angeles (Nov. 17, 1997).

Sambramurthi, J. K., and A. Alvarado, "Correlation of Slag Expulsion with Ballistic Anomalies in Shuttle Solid Rocket Motors," *AIAA J. Propulsion Power*, **12**(3), 598 (1996); Beiting, *AIAA J. Spacecraft and Rockets*, **34**(3), 303 (1997).

Samson, R. J., G. W. Mulholland, and J. W. Gentry, "Structural Analysis of Soot Agglomerates," *Langmuir*, **3**, 272 (1987).

Sorensen, C., J. Cai, and N. Lu, "Light Scattering Measurements of Monomer Size, Monomers per Aggregate, and Fractal Dimension for Soot Aggregates in Flames," *Appl. Optics*, **31**, 6547 (1992).

Tandon, P., and D. E. Rosner, "Monte-Carlo Simulation of Fractal Particle Aggregation and Restructuring," *J. Colloid Int. Sci.*, in press (1997).

Tandon, P., and D. E. Rosner, "Sintering Kinetics and Transport Property Evolution of Large Multi-Particle Aggregates," *Chem. Eng. Comm.*, **151**, 147 (1996).

Tandon, P., and D. E. Rosner, "Translational Brownian Diffusion Coefficient of Large (Multi-particle) Suspended Aggregates," *I/EC-Res. (ACS)*, **34**, 3265 (1995).

Tandon, P., "Transport Theory for Particles Generated in Combustion Environments," PhD Diss., Dept. of Chemical Engineering, Yale Univ. (May, 1995).

Ulrich, G. D., "Flame Synthesis of Fine Particles," *Chem. Eng. News (ACS)*, **62**(32), 22 (1984).

Wu, M., and S. K. Friedlander, "Enhanced Power-Law Agglomerate Growth in the Free-Molecule Regime," *J. Colloid Int. Sci.*, **159**, 246 (1993).

Xing, Y., Ü. Ö. Köylü, and D. E. Rosner, "Synthesis and Restructuring of Inorganic Nano-particles Particles in Counterflow Diffusion Flames," *Comb. & Flames*, **107**, 85 (1996a).

Xing, Y., P. Tandon, Ü. Ö. Köylü, and D. E. Rosner, "Experimental and Theoretical Studies of the Structure of Inorganic Particle-Producing Seeded Laminar Counterflow Diffusion Flames," Paper 59p, AIChE Meeting, Miami Beach, FL (Nov., 1995).

Xing, Y., P. Tandon, Ü. Ö. Köylü, and D. E. Rosner, "Measuring and Modelling the Synthesis and Morphological Evolution of Particles in Laminar Counterflow Diffusion Flames," *Extended Abstract in Proc. World Cong. of Chem. Eng.*, Paper No. 88d, Vol. V, San Diego, CA (July 14–18, 1996b).

Xing, Y., and D. E. Rosner, "Surface Melting of Particles: Predicting Spherule Size in Vapor Phase Nanometer Particle Synthesis," Paper No. V5.36, MRS Proc. 457, Fall 1996 MRS Meeting, Boston, MA, pp. 169–172 (1997).

Xing, Y., D. E. Rosner, and Ü. Ö. Köylü, "Light Scattering Measurements of Inorganic Aerosol Restructuring in Flames," AAAR, Denver, CO, Paper 10CA, in press (1997).

Xing, Y., "Synthesis and Morphological Evolution of Inorganic Nano-particles in Gas Phase Flames," PhD Diss., Dept. of Chemical Engineering, Yale Univ. (Sept., 1997).

Xiong, Y., and S. E. Pratsinis, "Gas Phase Production of Particles in Reactive Turbulent Flows," *J. Aerosol Sci.*, **24**(3), 283 (1993); *J. Aerosol Sci.*, **22**(5), 637 (1991).

Zacharaiah, M., and H. G. Semerjian, "Simulation of Ceramic Particle Formation: Comparison with *In Situ* Measurements," *AIChE J.*, **35**(12), 2003 (1989); see also Zachariah, M. R., D. Chin, H. G. Semerjian, and J. L. Katz, *Comb. & Flame*, **78**, 287 (1989).

Manuscript received Oct. 28, 1996, and revision received July 3, 1997.